Coupled core-mantle thermal evolution of early Mars

Y. Ke[1] and V. S. Solomatov[1]

Received 5 November 2008; revised 23 April 2009; accepted 5 May 2009; published 18 July 2009.

[1] Several arguments point out that at the end of planetary accretion, the core of Mars was likely to be much hotter than its mantle, resulting in the formation of a completely or partially molten thermal boundary layer at the base of the mantle. Here we address the following questions: How did the superheated core cool and what role did it play in the early mantle dynamics of Mars? We divide the coupled core-mantle evolution of early Mars into two stages. During the first stage, vigorous convection within the molten boundary layer removes the heat from the core so that the boundary layer expands up. As the boundary layer gets thicker, the temperature of the layer decreases. Eventually, the temperature of the molten boundary layer drops down to the temperature for the rheological transition (melt fraction ~40%) within 100 years. This stage is described by a parameterized convection approach. The second stage is modeled in spherical shell geometry using the fully three-dimensional finite element code CitcomS. A single plume ("superplume") forms by the instability of the thermal boundary layer. The superplume stage lasts much longer, on the scale of millions to hundreds of millions of years, depending on the mantle viscosity. During both stages of evolution the heat flux can easily satisfy the requirements for the dynamo.

Citation: Ke, Y., and V. S. Solomatov (2009), Coupled core-mantle thermal evolution of early Mars, *J. Geophys. Res.*, *114*, E07004, doi:10.1029/2008JE003291.

1. Introduction

[2] Various arguments suggest that the mantles of the terrestrial planets were partially or completely molten during accretion [e.g., *Elkins-Tanton et al.*, 2003, 2005a, 2005b; *Solomatov*, 2007]. The energy associated with large impacts and core formation are among the most significant factors contributing to heating and melting of the mantle. The cores of the terrestrial planets may have been even hotter than their mantles [*Ke and Solomatov*, 2006]. This possibility is supported by several arguments. On the present-day Earth, the temperature contrast between the lower mantle and the core is estimated to be 1000 to 2000 K [*Boehler*, 1996, 2000; *Williams*, 1998] and was probably even higher in the past as the core temperature must have decreased more than the mantle temperature during planetary evolution [*Stevenson et al.*, 1983]. Another argument comes from numerical simulations of giant impacts, which show that during collisions of large differentiated bodies with the proto-Earth the material that was heated most was the iron core of the impactor [*Canup*, 2004]. After the iron from the impactor's core segregated into the Earth's core, the temperature contrast between the core and the mantle reached several thousand degrees Kelvin. For a smaller planet like Mars the core-mantle temperature difference after a giant impact may be high as well, of the order of ~1000 K [*Ke and Solomatov*, 2006].

[3] A different argument for a superheated core was suggested by *Stevenson* [2001]. He pointed out that a substantial fraction of the gravitational potential energy of core formation can, in principle, be retained within the segregated iron. Although there are many factors controlling the energy partitioning between the mantle and the core, how liquid iron moves through the dominantly solid mantle might be the most important one.

[4] If liquid iron moves through the mantle in the form of blobs, the mantle has to deform to allow the motion of the blobs (Figure 1a). Because the strain rates in the liquid iron, $\dot{e}_{\mathrm{Fe}}$, and the mantle, $\dot{e}_{\mathrm{m}}$, are of the same order of magnitude (this is valid when the blob viscosity is smaller than the viscosity of the surrounding fluid, see the solution for the flow around a sphere with finite viscosity [*Landau and Lifshitz*, 1987]), the ratio of viscous dissipation rates between the iron and the mantle is proportional to

$$\frac{\dot{\epsilon}_{\mathrm{Fe}}}{\dot{\epsilon}_{\mathrm{m}}} = \frac{\mu_{\mathrm{Fe}}\dot{e}_{\mathrm{Fe}}^2}{\mu_{\mathrm{m}}\dot{e}_{\mathrm{m}}^2} \propto \frac{\mu_{\mathrm{Fe}}}{\mu_{\mathrm{m}}}, \tag{1}$$

where μ_{m} is the mantle viscosity and μ_{Fe} is liquid iron viscosity. This means that most of the gravitational potential energy of core formation dissipates within the mantle (Figure 1a).

[5] Numerical simulations show that magma migration [*Wiggins and Spiegelman*, 1995; *Connolly and Podladchikov*, 2007] as well as segregation of liquid iron [*Golabek et al.*, 2008] results in the formation of melt channels. If liquid

[1]Department of Earth and Planetary Sciences, Washington University, St. Louis, Missouri, USA.

0148-0227/09/2008JE003291

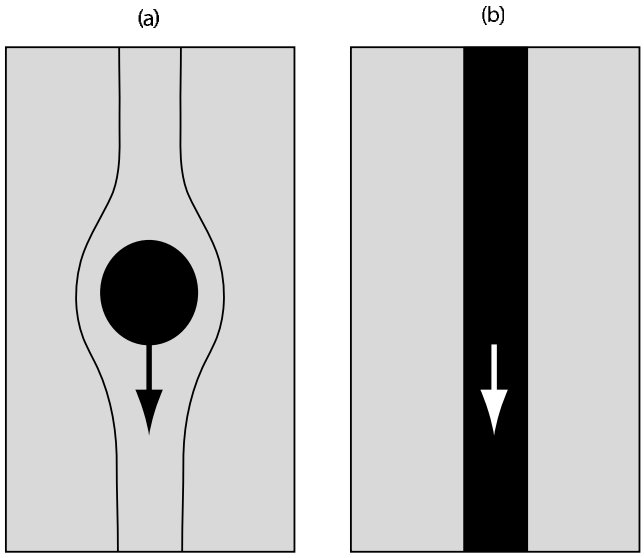

Figure 1. Two end-member cases of iron segregation in the Martian mantle: (a) low-viscosity liquid iron blobs sink through a viscous mantle (the streamlines of the mantle flow around the blob are shown schematically) and (b) liquid iron flows down in cracks or channels. In Figure 1a, viscous dissipation is largest in the mantle. In Figure 1b, viscous dissipation is largest in the channel.

iron segregated in channels (Figure 1b), then the viscous stresses in the liquid iron, τ_{Fe}, and in the mantle, τ_{m}, are of the same order of magnitude and thus, the ratio of viscous dissipation rate between the iron and the mantle is

$$\frac{\dot{\epsilon}_{\mathrm{Fe}}}{\dot{\epsilon}_{\mathrm{m}}} = \frac{\tau_{\mathrm{Fe}}^2/\mu_{\mathrm{Fe}}}{\tau_{\mathrm{m}}^2/\mu_{\mathrm{m}}} \propto \frac{\mu_{\mathrm{m}}}{\mu_{\mathrm{Fe}}}. \tag{2}$$

This implies that if iron segregated in channels the energy of core formation would largely go into the core ($\mu_{\mathrm{m}} \gg \mu_{\mathrm{Fe}}$).

[6] Assuming that Mars was initially homogeneous, *Solomon* [1979] estimated that the gravitational potential energy released by core formation is $\Delta\Omega \sim 2 \times 10^{29}$ J. If all this energy is used to heat up the core, the average core temperature increases by

$$\Delta T_c = \frac{\Delta\Omega}{M_c c_{pc}} \approx 1800 \text{ K}, \tag{3}$$

where $M_c \approx 1.4 \times 10^{23}$ kg is the mass of the core and $c_{pc} \approx 800$ J kg^{-1} K^{-1} is the specific heat of the core (Table 1).

[7] If we consider the effect of a single giant impact, then assuming that the impact is about 0.1 of the mass of proto-Mars we obtain that segregation of iron from such an impact raises the core temperature by

$$\Delta T_c' \sim 0.1 \frac{gH}{c_{pc}} \approx 500 \text{ K}, \tag{4}$$

where $g = 3.7$ m s^{-2} is the gravity and $H \sim 1000$ km is the thickness of the Martian mantle (Table 1). The above estimates should be considered as an upper bound because some fraction of the heat, depending on the channel width and other factors, escapes from the hot channels to the mantle.

[8] In addition to core superheating, an overturn of the Martian mantle would adiabatically cool the lower part of the mantle and increase the core-mantle temperature contrast even further. According to *Elkins-Tanton et al.*'s [2005a] calculations, the core-mantle temperature contrast due to mantle overturn is on the order of $\Delta T_m \sim 1000$ K.

[9] The three effects described above, (1) the shock wave heating of impactor's iron core, (2) the predominant partitioning of the core formation energy into the core, and (3) lower mantle cooling due to mantle overturn, together may generate the temperature contrast between the core and the lower part of the Martian mantle from several hundred to several thousand degrees Kelvin.

[10] This raises the following questions: How did the Martian core cool and what role did it play in the early evolution of the mantle? In our previous study we showed that a superheated core is likely to generate a single transient superplume which may be responsible for the formation of the Martian crustal dichotomy [*Ke and Solomatov*, 2006]. Here, we consider a coupled evolution of the core-mantle system and provide some constraints on how rapidly the core cools, what controls the cooling rate, how the decreasing temperature of the core affects the superplume evolution, and whether and for how long this type of dynamics can provide energy for the generation of the magnetic field on early Mars. We should note that while our discussion focuses on Mars, the results are general and can be applied to other planets as well.

2. Model

[11] We consider a highly simplified structure of the mantle and the core immediately after the segregation of hot iron. The Martian mantle is assumed to be a spherical shell with uniform density ρ_m, temperature T_m, viscosity μ_m, and thickness $H = R_p - R_c$, where R_c is the core radius and

Table 1. Physical Parameters

Parameter	Value	Reference[a]
Gravity, g	3.7 m s^{-2}	1
Planetary radius, R_p	3390 km	1
Mantle density, ρ	4000 kg m^{-3}	1
Core radius, R_c	1700 km	2
Core mass, M_c	1.4×10^{23} kg	3
Pressure at CMB, P_{CMB}	23 GPa	3
Mantle specific heat, C_{pm}	1200 J kg^{-1} K^{-1}	1
Core specific heat, C_{pc}	800 J kg^{-1} K^{-1}	4
Latent heat, L	5×10^5 J kg^{-1}	4
Thermal expansion, α	2×10^{-5} K^{-1}	5
Thermal conductivity, k	4 W m^{-1} K^{-1}	6
Reference viscosity (solid), $\mu_{0,s}$	4.27×10^{10} Pa s	7
Activation energy (solid), E_s	240 kJ mol^{-1}	7
Activation volume (solid) V_s	5×10^{-6} m^3 mol^{-1}	7
Reference viscosity (liquid), $\mu_{0,l}$	10^{-5} Pa s	8
Activation energy (liquid), E_l	195 kJ mol^{-1}	8
Activation volume (liquid), V_l	-3.65×10^{-6} m^3 mol^{-1}	8

[a] 1, *Zharkov* [1986]; 2, *Yoder et al.* [2003]; 3, *Longhi et al.* [1992]; 4, *Anderson* [1995]; 5, *Chopelas* [1996]; 6, *Hofmeister* [1999]; 7, *Karato and Wu* [1993]; 8, *Liebske et al.* [2005].

R_p is the planet radius. Any variations in mantle properties are assumed to be negligible compared to the difference between the mantle and the hot thermal boundary layer (TBL) formed at the core-mantle boundary (CMB). If a partially molten shallow layer (a shallow magma ocean) existed at that time, it would mechanically decouple the lithosphere from the deep mantle. In this case the upper boundary of our model mantle corresponds roughly to the depth at which the melt fraction is ~40% (which is roughly the rheological transition between liquid-like and solid-like behavior, see below). The upper and the bottom boundaries of the mantle are stress-free.

[12] The mantle temperature T_m during planetary accretion was probably not far from the mantle solidus. If the mantle was ever significantly molten, vigorous convection would cool the mantle very fast to near-solidus temperatures [*Williams and Nimmo*, 2004]. At the CMB pressure the solidus temperature is around 2450 K [*Zhang and Herzberg*, 1994]. This is an upper bound on the initial mantle temperature T_m. Depending on the mantle composition and the details of the mantle temperature profile, at this temperature the partially molten shallow layer may occupy a substantial portion of the mantle. A lower bound can be obtained by requiring the mantle to be completely solid which gives $T_m \approx 1600$ K. We also assume that radiogenic heating can be ignored owing to differentiation of incompatible elements into the crust and/or owing to short time scales considered in this study.

[13] The Martian core is assumed to be vigorously convecting and have an adiabatic temperature profile with the CMB temperature higher than the mantle temperature by ΔT, that is $T_{\rm CMB} = T_m + \Delta T$. For $T_m = 1600-2400$ K and $\Delta T = 1000$ K, $T_{\rm CMB} = 2600-3400$ K. This suggests that $T_{\rm CMB}$ can easily exceed both the solidus (~2450 K) and the liquidus (~2650 K) [*Zhang and Herzberg*, 1994]. Although the uncertainties in these estimates are large, it seems very likely that the mantle was substantially molten and a completely or partially molten layer formed at the base of the mantle.

[14] The processes in the partially molten layer formed near the core-mantle boundary can be quite complicated [*Labrosse et al.*, 2007] and similar to those occurring in magma oceans formed in the upper parts of planetary mantles [*Solomatov and Stevenson*, 1993a, 1993b; *Solomatov*, 2000, 2007]. We assume that only negligible crystal melt segregation occurs during cooling and crystallization of the molten region near the core-mantle boundary. The validity of this assumption depends on the crystallization time of the molten layer at the Martian core-mantle boundary and the crystal size. We will show the crystallization time is of the order of 100 years. This is sufficiently fast to ignore crystal melt segregation in the terrestrial magma ocean provided the crystals are less than 1 mm in diameter [*Solomatov*, 2000, 2007]. Similar arguments apply to the Martian partially molten layer at the core-mantle boundary. Given huge uncertainties, both equilibrium crystallization scenario and fractional crystallization scenario of the molten layer seem equally possible. We will be assume the former as the simplest of the two. During plume formation, segregation of melt may become faster than the crystallization time. It would be interesting to consider the effect of melt segregation on plume formation in the future.

[15] Qualitatively the system evolves as follows. Initially, most of the TBL is substantially molten and convection within the TBL is very vigorous. As the TBL thickness increases with time, both the TBL temperature and the core temperature decrease. At melt fraction $\phi = \phi_{cr} = 40\%$ (or crystal fraction 60%) the partially molten system undergoes a rheological transition from a low-viscosity crystal suspension (that is the viscosity is controlled by liquid viscosity) to a partially molten solid (that is the viscosity is controlled by the deformation of the solid phase). The dynamic processes become much slower and are dominated by the large-scale instability of the TBL-mantle system.

[16] Because no numerical code can handle the enormous viscosity contrast between the liquid and solid parts of the mantle, we first use a parameterized convection approach to describe the cooling of the TBL and the core before the melt fraction in the TBL drops below the rheological transition. Then we apply a fully three-dimensional finite element code CitcomS [*Zhong et al.*, 2000] to calculate the evolution beyond the rheological transition.

3. First Stage of Evolution: Parameterized Convection Calculations

3.1. Energy Balance Equation for the Core

[17] The energy balance equation for the core is

$$c_{pc} M_c \frac{d\overline{T}_c}{dt} = -A_c F_c, \tag{5}$$

where $\overline{T}_c$ is the average temperature of the core, F_c is the heat flux at the CMB, $M_c = (4\pi/3)\rho_c R_c^3$ is the mass of the core, ρ_c is the core density, and A_c is the surface area of the core.

[18] Assuming that the core is liquid and is vigorously convecting we can relate its average temperature $\overline{T}_c$ to the temperature $T_{\rm CMB}$ of the core-mantle boundary:

$$\overline{T}_c = \beta T_{\rm CMB}, \tag{6}$$

where $\beta \approx 1.1$ [*Stevenson et al.*, 1983]. We obtain

$$\frac{dT_{\rm CMB}}{dt} = -\frac{3F_c}{\beta \rho_c c_{pc} R_c}. \tag{7}$$

[19] The above formulae assume that the core is well mixed. Another assumption is that the temperature difference across the thermal boundary layer on the core side of the CMB is negligible. This boundary layer would substantially affect the estimates of the CMB heat flux and the TBL crystallization time only if the viscosity of liquid iron is much larger than the viscosity of liquid silicates, which seems unlikely [*Liebske et al.*, 2005; *Mound and Buffett*, 2007].

3.2. Energy Balance Equation for the TBL

[20] To write the energy balance equation for the TBL we need to take into account the heat flux into the TBL, the

heat flux out of the TBL, the temperature change of the TBL, the change in the thickness of the TBL and the latent heat of crystallization if there is any melt present. The heat flux into the TBL is equal to the heat flux F_c from the core. The heat flux out of the TBL (at the upper boundary) is close to zero because the temperature profile above the TBL quickly reaches a steady state profile in the frame of reference associated with the moving upper boundary of the TBL [*Solomatov and Moresi*, 2002]. The amount of heat stored in the TBL changes mainly because of the increase in the thickness of the TBL and the simultaneous decrease of its nearly isothermal convective interior. The latter is caused by the decrease in the core temperature and the fact that the temperature difference between the CMB temperature and the temperature of the nearly isothermal convective interior of the TBL is nearly constant and controlled by the rheological temperature difference [*Solomatov and Moresi*, 2002]. The energy balance for the partially molten TBL with the time-dependent thickness $h(t)$ and the melt fraction $\phi_{\mathrm{TBL}}(t)$ of the interior of the TBL is described by the following energy balance equation:

$$\frac{d}{dt}\left\{M_h\left[c_{pm}(T_{\mathrm{TBL}}-T_m)+\phi_{\mathrm{TBL}}L\right]\right\}=A_cF_c, \tag{8}$$

where c_{pm} is the specific heat of the mantle, $M_h = (4\pi/3)\rho_m[(R_c+h)^3 - R_c^3]$ is the mass of the TBL, L is the latent heat, and T_{TBL} is the interior temperature of the TBL.

[21] In linear approximation, the melt fraction is

$$\phi_{\mathrm{TBL}}=\frac{T_{\mathrm{TBL}}-T_s}{T_l-T_s}, \tag{9}$$

where T_l and T_s are mantle liquidus and solidus temperatures respectively.

3.3. Parameterized Convection Calculations

[22] Equations (7) and (8) can be integrated to obtain h:

$$h=R_c\left\{\left[\left(\frac{\rho_c}{\rho_m}\right)\frac{c_{pc}\beta\left(T^0_{\mathrm{CMB}}-T_{\mathrm{CMB}}\right)}{c_{pm}(T_{\mathrm{TBL}}-T_m)+\phi_{\mathrm{TBL}}L}+1\right]^{1/3}-1\right\}, \tag{10}$$

where T^0_{CMB} is the initial CMB temperature. The initial thickness of the TBL is assumed to be zero.

[23] To find h as a function of time and estimate the crystallization time of the TBL we need to integrate equations (7) and (8) with respect to time. However, because we already have equation (10) we only need to integrate equation (7). This integration requires the function F_c and the relationship between T_{TBL} and T_{CMB}.

[24] For either turbulent or laminar convection and constant viscosity or strongly temperature-dependent viscosity convection, the heat flux F_c can be approximately parameterized as follows [*Kraichnan*, 1962; *Siggia*, 1994; *Schubert et al.*, 2001; *Solomatov*, 1995; *Solomatov and Moresi*, 2000]:

$$F_c\approx a_c k\Delta T_c^{4/3}\left(\frac{\alpha\rho_m g}{\kappa\mu_{\mathrm{TBL}}}\right)^{1/3}, \tag{11}$$

where k is the thermal conductivity, κ is the thermal diffusivity, α is the thermal expansivity, and μ_{TBL} is the viscosity of the convective interior of the TBL. The coefficient a_c and the driving temperature ΔT_c depend on the convective regime, heating mode and boundary conditions. The coefficient a_c varies very little and is usually close to $\sim$0.1. We will use $a_c = 0.12$ in all our calculations.

[25] The driving temperature difference ΔT_c varies substantially with temperature. When the temperature is very high (several thousand degrees Kelvin), and thus the interior of the TBL is completely molten, the viscosity variations are relatively small (at least in the temperature range from T_l to $T_{\mathrm{CMB}} > T_l$) and convection can be considered as constant viscosity convection with $\Delta T_c \approx T_{\mathrm{CMB}} - T_{cr}$, where T_{cr} is the critical temperature for the rheological transition.

[26] At lower temperatures the viscosity depends strongly on temperature, and the driving temperature difference is proportional to the rheological temperature scale $\Delta T_{rh} = \left|d\ln\mu/dT\right|^{-1}$ [*Morris and Canright*, 1984; *Fowler*, 1985; *Davaille and Jaupart*, 1993a; *Solomatov*, 1995; *Moresi and Solomatov*, 1995; *Trompert and Hansen*, 1998]:

$$\Delta T_c\approx 3\Delta T_{rh}. \tag{12}$$

For a partially molten system, the rheological temperature scale is defined as follows [*Davaille and Jaupart*, 1993b; *Reese and Solomatov*, 2006]:

$$\Delta T_{rh}=\left|\frac{d\ln\mu(T,\phi(T))}{dT}\right|^{-1}, \tag{13}$$

where $\mu(T, \phi(T))$ is an experimentally determined function of temperature T and melt fraction $\phi(T)$ and the partially molten system is assumed to be in thermodynamic equilibrium (otherwise ϕ would be history-dependent).

[27] The viscosity of concentrated suspensions can be estimated using Roscoe's formula [*Roscoe*, 1952] (for alternative formulae see [*Solomatov and Stevenson*, 1993a]):

$$\mu_{pm,\phi>\phi_{cr}}=\mu_l\left(\frac{1-\phi_{cr}}{\phi-\phi_{cr}}\right)^{2.5}, \tag{14}$$

where the viscosity of pure liquid is

$$\mu_l=\mu_{0,l}\exp\left(\frac{Q_l}{RT}\right)=\mu_{0,l}\exp\left(\frac{E_l+PV_l}{RT}\right), \tag{15}$$

where $\mu_{0,l}$ is a constant, Q_l, E_l, and V_l are the activation enthalpy, the activation energy, and the activation volume, respectively [e.g., *Liebske et al.*, 2005].

[28] Using equations (9), (13), (14), and (15) we obtain

$$\Delta T_{rh}=\left(\frac{Q_l}{RT^2_{\mathrm{TBL}}}+\frac{2.5}{T_{\mathrm{TBL}}-T_{cr}}\right)^{-1}. \tag{16}$$

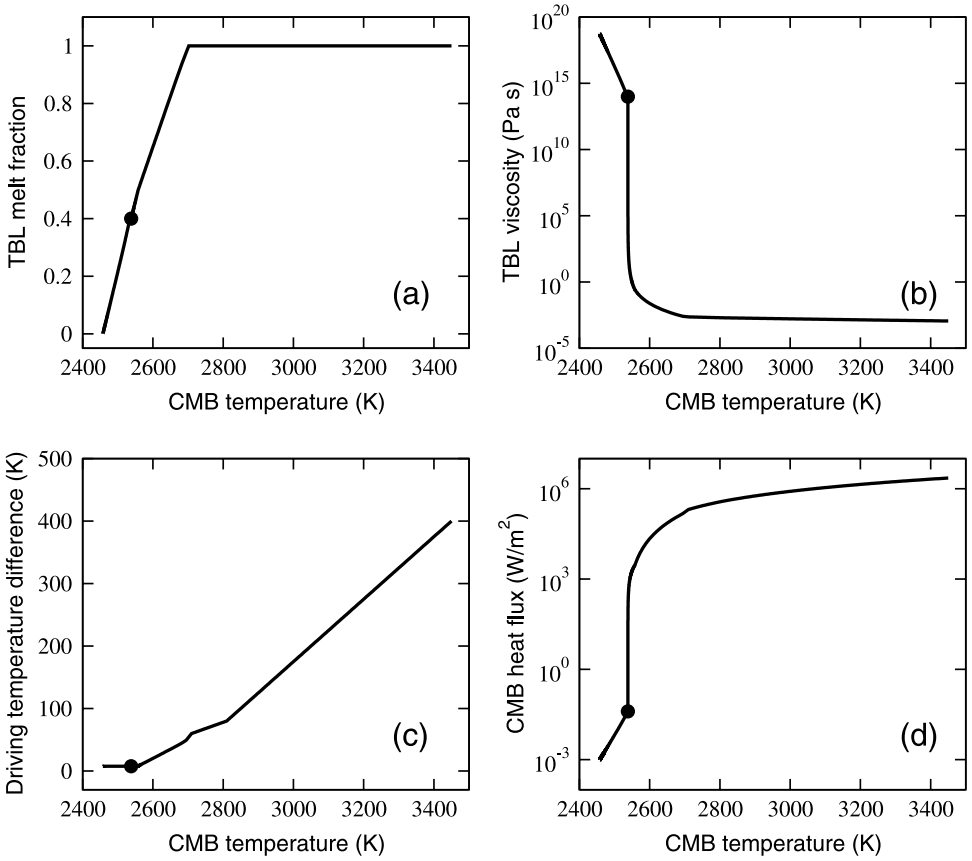

Figure 2. (a) Melt fraction in the thermal boundary layer (TBL; at $T = T_{\mathrm{TBL}}$), (b) the viscosity of the TBL, (c) the temperature difference between the core-mantle boundary (CMB) and the TBL, and (d) the heat flux at the CMB as functions of the CMB temperature. As the temperature increases the deformation mechanism changes from a purely solid state creep to solid state creep softened by the presence of small amounts of melt (at $\phi < \phi_{cr}$), to viscosity of partial melts at high melt fractions ($\phi > \phi_{cr}$), and finally to purely liquid viscosity. The rheological transition at $\phi = \phi_{cr} = 40\%$ is shown with a black circle.

At low melt fractions we can use the solid state viscosity reduced owing to the presence of melt:

$$\mu_{pm,\phi<\phi_{cr}} = \mu_s \exp(-\alpha_\mu \phi), \tag{17}$$

where $\alpha_\mu \sim 25$ for diffusion creep [*Scott and Kohlstedt*, 2004] and μ_s is the viscosity of solid silicates:

$$\mu_s = \mu_{0,s} \exp\left(\frac{Q_s}{RT_{\mathrm{TBL}}}\right) = \mu_{0,s} \exp\left(\frac{E_s + PV_s}{RT_{\mathrm{TBL}}}\right), \tag{18}$$

where $\mu_{0,s}$ is constant, Q_s, E_s, and V_s are the activation enthalpy, the activation energy, and the activation volume, respectively [*Karato and Wu*, 1993]. In this case, the rheological temperature scale is

$$\Delta T_{rh} = \left(\frac{Q_s}{RT_{\mathrm{TBL}}^2} + \frac{\alpha_\mu}{T_l - T_s}\right)^{-1}. \tag{19}$$

To smooth the transition between the two regimes, $\phi > \phi_{cr}$ and $\phi < \phi_{cr}$, we use the following equation:

$$\frac{1}{\mu_{pm}} = \frac{1}{\mu_{pm,\phi>\phi_{cr}}} + \frac{1}{\mu_{pm,\phi<\phi_{cr}}}. \tag{20}$$

[29] Because a secondary thermal boundary layer forms at the bottom of the vigorously convecting TBL, the TBL temperature T_{TBL} is smaller than the CMB temperature T_{CMB}. At high temperatures, when the TBL can be treated as a nearly isoviscous layer, we assume that $T_{\mathrm{CMB}} - T_{\mathrm{TBL}} \approx 0.5\Delta T_c$. At lower temperatures we can use the stagnant lid convection scaling $T_{\mathrm{CMB}} - T_{\mathrm{TBL}} \approx \Delta T_{rh}$. To smooth the transitions between all the regimes we simply require that $T_{\mathrm{CMB}} - T_{\mathrm{TBL}}$ monotonically increases with T_{CMB}.

[30] Figure 2 shows variations of the TBL parameters with the CMB temperature. As the CMB temperature decreases from liquidus (T_l = 2650 K) to solidus (T_s = 2450 K), the driving temperature difference for convection inside the TBL decreases, the viscosity increases and the heat flux decreases. The most drastic changes occur around $\phi \sim \phi_{cr}$ ($T_{cr} \approx 2530$ K).

[31] Figure 3 shows the results of parameterized calculations of thermal evolution of the coupled core-mantle system for T_m = 1600, 2000 and 2400 K and $T_{\mathrm{CMB}} = T_m + 1000$ K. Cooling and crystallization of the molten TBL to $\phi = \phi_{cr}$ is very fast (~100 years) and depends only weakly on the assumed parameters. This fast time scale is due to a low viscosity of the TBL which generates a very

high convective heat flux as suggested by equation (11). After the melt fraction drops to ~40% (the end of the calculations in Figure 3) the viscosity significantly increases and the CMB temperature continues to decrease at a much slower rate.

3.4. TBL Thickness at the Rheological Transition

[32] When the TBL undergoes the rheological transition the viscosity contrasts in the mantle drop substantially and can be handled by fully three-dimensional finite element calculations. The TBL thickness and the temperatures of the core and the mantle at this transition can be used as a guide to choose the initial conditions for the three-dimensional calculations.

[33] To estimate $h = h_{cr}$ at the rheological transition, we require that $T_{\rm TBL} = T_{cr}$ and $\phi_{\rm TBL} = \phi_{cr}$. The CMB temperature $T_{\rm CMB}$ can be set to $T_{\rm CMB} \approx T_{cr}$ as well because the temperature difference between $T_{\rm CMB}$ and $T_{\rm TBL}$ becomes very small when $T_{\rm TBL}$ approaches T_{cr} (Figure 2c). The value of h_{cr} at the rheological transition is shown as a function of $T^0_{\rm CMB}$ and T_m in Figure 4.

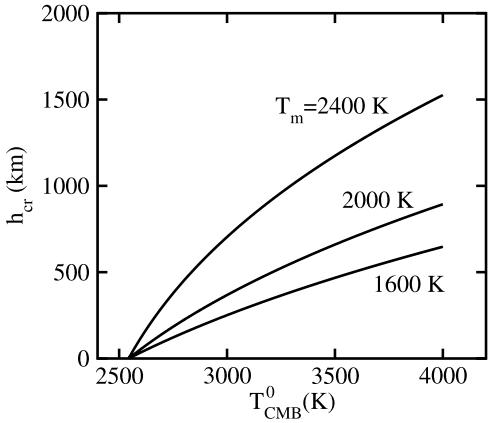

Figure 4. The thickness h_{cr} of the TBL by the time when the melt fraction in the TBL drops to ϕ_{cr} = 40% as a function of the initial CMB temperature $T^0_{\rm CMB}$. The temperature difference between the CMB and the TBL is assumed to be negligible at $\phi \sim \phi_{cr}$.

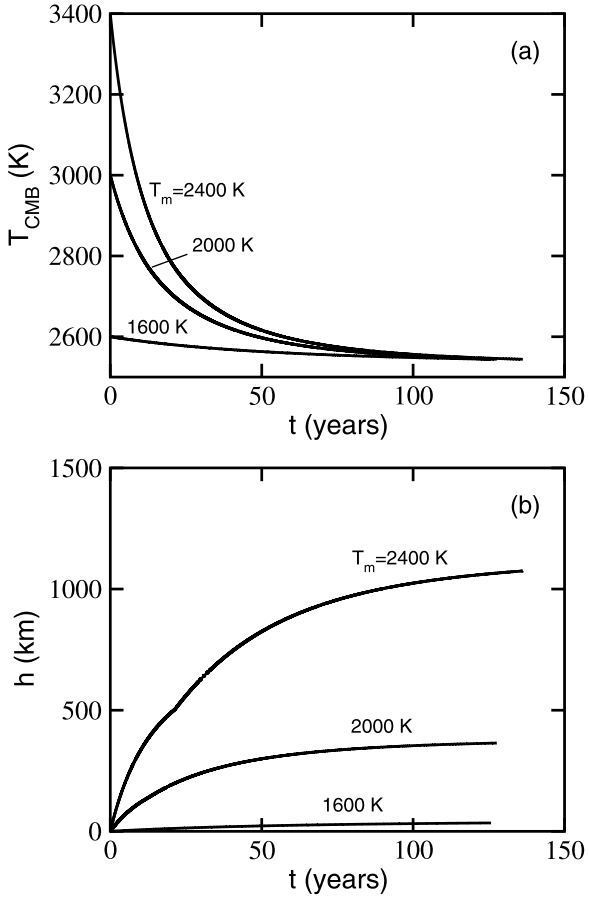

Figure 3. (a) Variation of the CMB temperature and (b) the thickness of the boundary layer during the first evolution stage when the behavior of the system is largely controlled by the viscosity of pure melt. The calculations end when the melt fraction drops to ϕ_{cr} = 40%. The labels show the mantle temperature. In all cases, the initial temperature of the CMB is higher than the mantle temperature by 1000 K.

4. Second Stage of Evolution: Fully Three-Dimensional Calculations

4.1. Equations

[34] To nondimensionalize the equations, we choose $H = R_p - R_c$ as the length scale, $t_0 = H^2/\kappa$ as the time scale, $u_0 = H/t_0$ as the velocity scale, and $\Delta T = T_{\rm CMB}(0) - T_m$ as the temperature scale, where $\kappa = k/(\rho_m c_{pm})$ is the coefficient of thermal diffusion and $T_{\rm CMB}(0) \approx T_{cr}$ is the initial temperature of the core-mantle boundary (in this section, "initial" refers to the initial conditions for the three-dimensional calculations). The ratio R_c/R_p is set to 0.5.

[35] Numerical simulations are performed using CitcomS [*Zhong et al.*, 2000]. The model is very similar to that studied by *Ke and Solomatov* [2006] except that we modified the code to take into account the effect of core cooling (equation (7)).

[36] The nondimensional equations of thermal convection in the Boussinesq approximation are

$$\nabla \times \mathbf{u} = 0, \tag{21}$$

$$0 = -\nabla p + \alpha \rho g T \mathbf{n} + \nabla \times \left[\mu\left(\nabla \mathbf{u} + \{\nabla \mathbf{u}\}^T\right)\right], \tag{22}$$

$$\frac{\partial T}{\partial t} + \mathbf{u} \times \nabla T = \nabla^2 T, \tag{23}$$

where $\mathbf{u}$ is the velocity vector, p and T are the pressure and temperature perturbations, $\mathbf{n}$ is a unit vector in the direction of gravity, and $\{\}^T$ is the transpose operator.

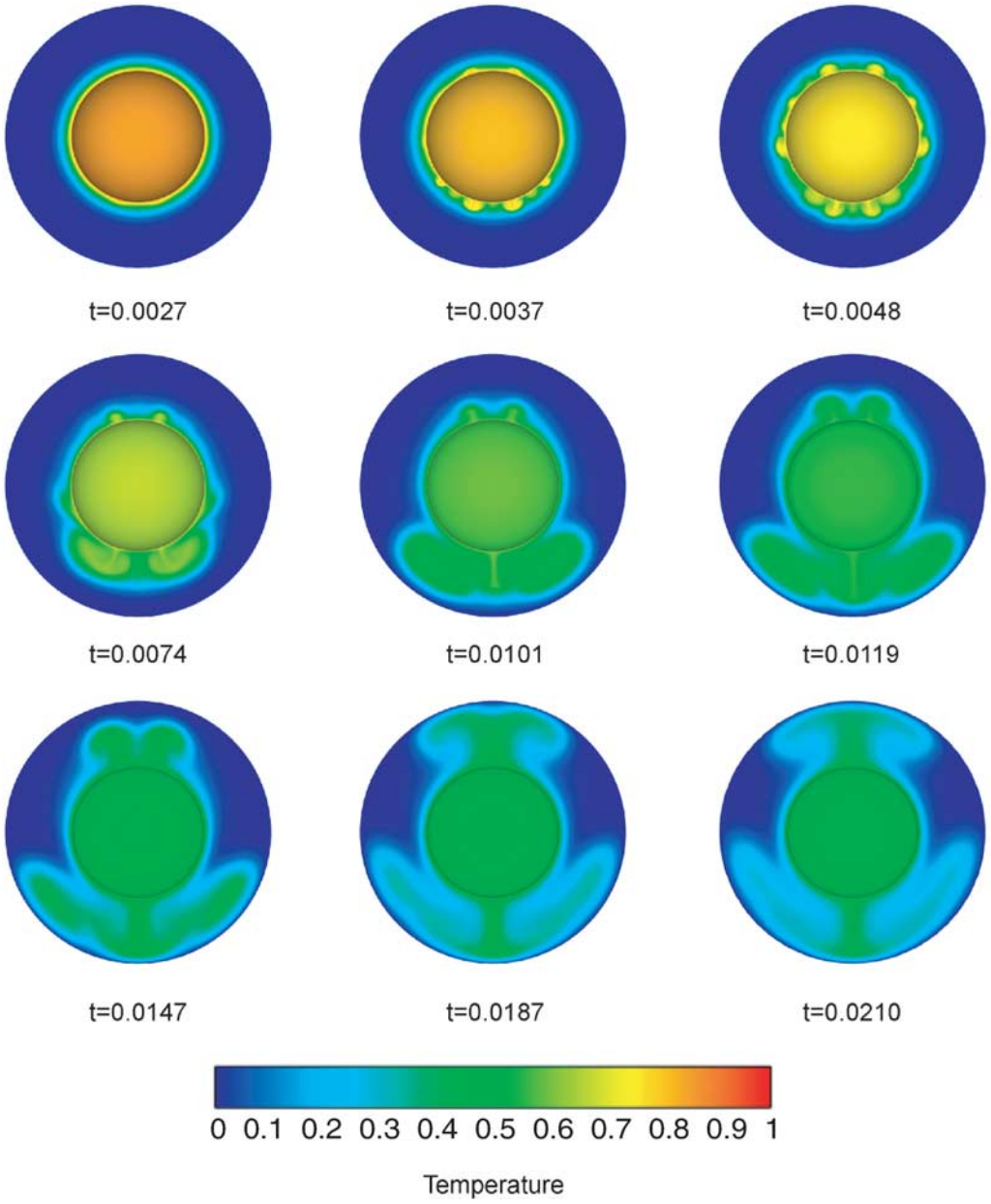

Figure 5. A sequence of snapshots (cross sections of the spherical shell temperature distribution) from fully three-dimensional simulations of superplume formation with core cooling. The central sphere shows the CMB surface. The initial boundary layer thickness is negligibly small, $h(0) \sim 0$. The nondimensional initial CMB temperature is $T_{\mathrm{CMB}} = 1$. It gradually decreases during superplume formation.

[37] The Rayleigh number is defined as

$$Ra_m = \frac{\alpha \rho_m g \Delta T H^3}{\kappa \mu_m}, \tag{24}$$

where α is the thermal expansion coefficient, g is the acceleration due to gravity, and μ_m is the mantle viscosity.

[38] The viscosity law used in the numerical calculations is as follows:

$$\mu = \mu_m \exp[-\gamma(T - T_m)], \tag{25}$$

where γ is a constant defining the contrast between the mantle viscosity μ_m and the viscosity μ_{CMB} at the core-mantle boundary

$$\frac{\mu_m}{\mu_{\mathrm{CMB}}} = \exp[\gamma(T_{\mathrm{CMB}} - T_m)]. \tag{26}$$

This viscosity law is clearly a simplification of the actual complex rheology of the TBL and the mantle as a whole. Our previous calculations [*Ke and Solomatov*, 2004, 2006] suggest that the details of the viscosity law may not be very important (like in many other cases involving strongly

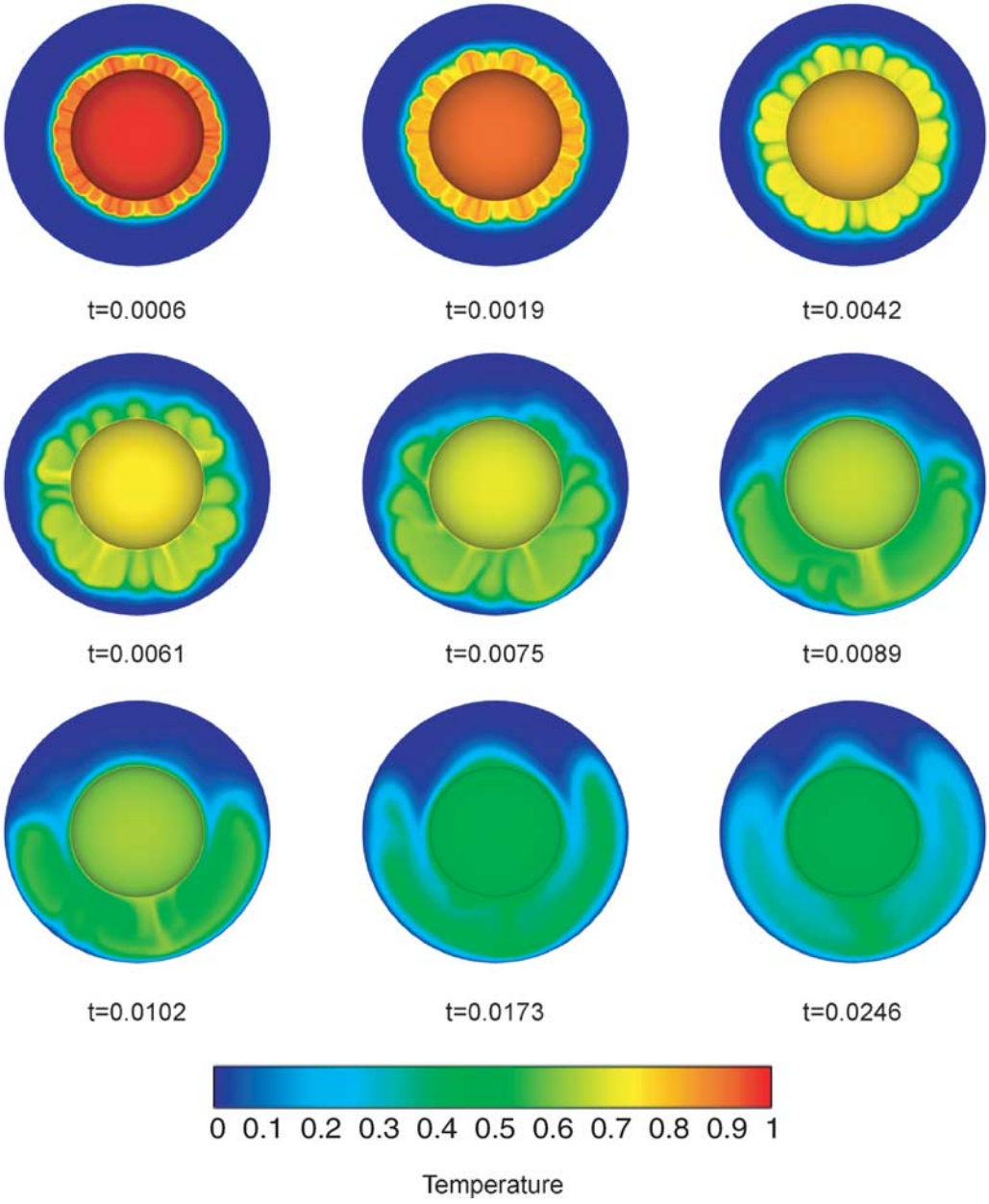

Figure 6. Same as Figure 5 but the initial boundary layer thickness is $h(0) = 0.25$.

temperature-dependent viscosity [e.g., *Solomatov*, 1995]). In our problem, two properties of the viscosity law matter most. One is the viscosity function of the least viscous region that is the convective region inside the TBL (where the viscosity varies from $\mu_{\rm CMB}$ to roughly 10 $\mu_{\rm CMB}$). It can be reasonably well approximated by an exponential function (the Frank-Kamenetskii approximation). The other property is the total viscosity contrast between the mantle and the TBL. This controls the instability of the TBL-mantle system.

[39] The initial thermal state of the planet is an isothermal mantle (an isothermal mantle in Boussinesq approximation corresponds to an adiabatic mantle) with a basal boundary layer of thickness h and temperature $T_{\rm CMB}$. This basal layer represents a partially solidified TBL (with $\phi \sim \phi_{cr}$) after the initial core cooling period.

4.2. Parameters

[40] In all our calculations, $Ra_m = 1.25 \times 10^3$ and $\eta_m/\eta_{\rm CMB}$ $\eta_{\rm CMB} = 10^6$. Our choice of the Rayleigh number and the viscosity contrast represents a practical limit that can be achieved at present with the total number of finite elements $64 \times 64 \times 64 \times 12$ (CitcomS divides the 3-D spherical shell into 12 caps; for each cap, the grid is $64 \times 64 \times 64$). Note that although the Rayleigh number for the mantle as a whole appears small, the effective Rayleigh number for convection inside the TBL reaches $\sim 10^9$ because the TBL viscosity is much lower than the mantle viscosity. This implies an extremely vigorous convection and very thin thermal boundary layers inside the TBL itself.

[41] For the values of the parameters that we choose in this study a single superplume is the preferred instability

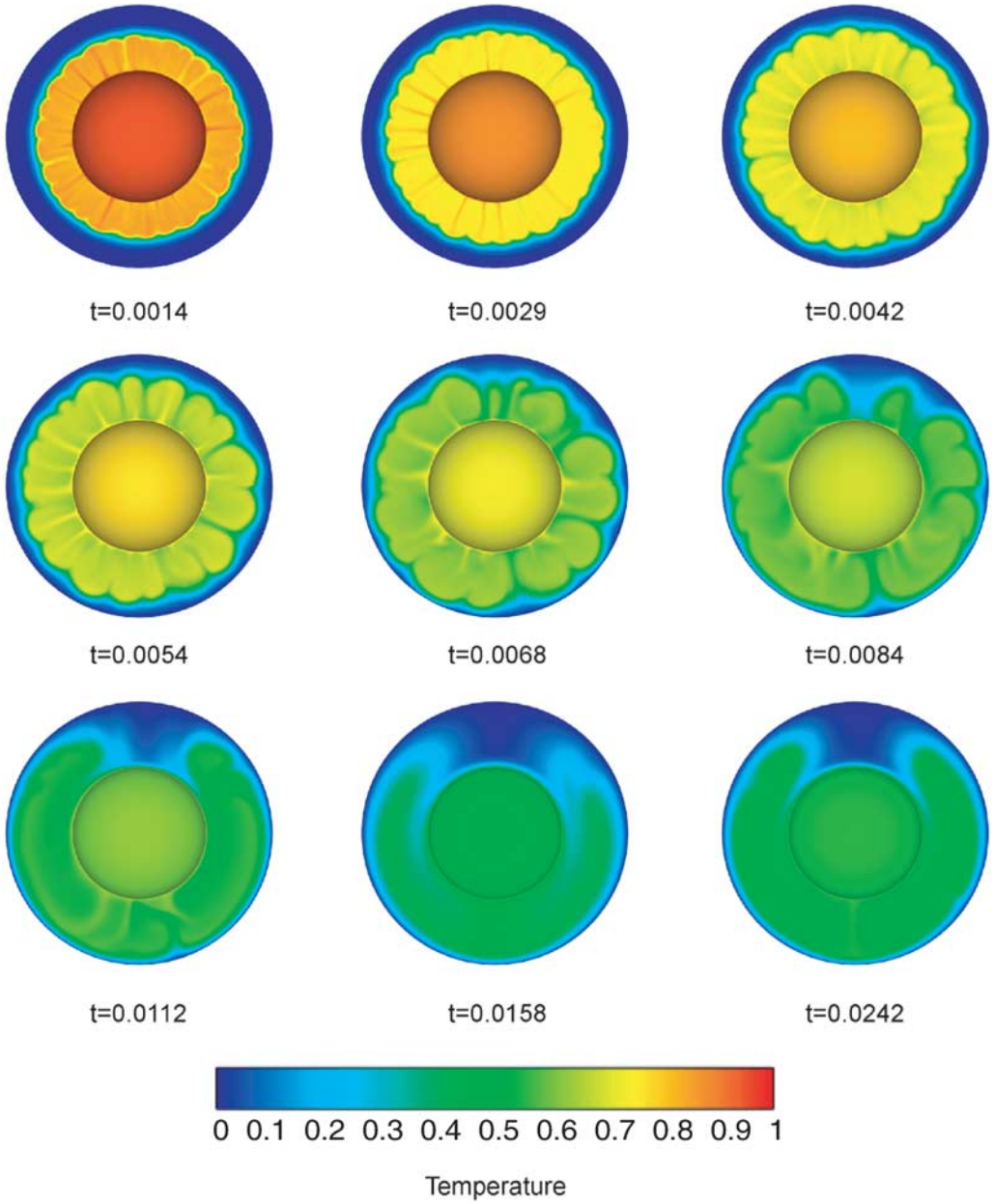

Figure 7. Same as Figure 5 but the initial boundary layer thickness is $h(0) = 0.5$.

mode (i.e., it grows faster than multiple plumes). The number of plumes depends on several parameters. *Ke and Solomatov* [2006] showed that at least in the linear theory of Rayleigh-Taylor instability in spherical geometry a single superplume forms if the viscosity contrast μ_m/μ_{TBL} between the mantle and the TBL is larger than $(R_c/h)^3$ (for $R_c/R_p \sim 0.5$) at the time when the superplume development becomes faster than the growth of the TBL. Because of a very short crystallization time of the TBL ($\Delta t \sim 10^2$ years, section 3.3), plumes do not form until the TBL reaches the rheological transition as long as the mantle viscosity is higher than $\sim\alpha\rho g\Delta T H\Delta t \sim 10^{18}$ Pa s (see equations (33) and (34) from [*Ke and Solomatov*, 2006]). Thus, a relatively modest viscosity contrast between the TBL (at the rheological transition) and the mantle is required to generate one superplume. For example, for $h \sim 100$ km, μ_m/μ_{TBL} has to be larger than $\sim(R_c/h)^3 \sim 5 \times 10^3$. This number is certainly smaller than the viscosity contrast between the near-solidus mantle and the mantle at the rheological transition. Thus, although it is possible to choose viscosity parameters that allow the formation of several plumes, we assume that the viscosity contrast between the TBL and the mantle is sufficiently large so that only a single superplume forms. On the basis of the results of parameterized convection calculations we consider a broad range of the initial nondimensional boundary layer thickness: $h(0) \sim 0$, 0.25, and 0.5.

4.3. Results

[42] The results of three-dimensional calculations are shown in Figures 5, 6, and 7. The coupled core-mantle thermal evolution can be divided into three stages: (1) the growth of the internally convecting thermal boundary layer, (2) the development of large-scale instability (the superplume formation), and (3) the spread and decay of the

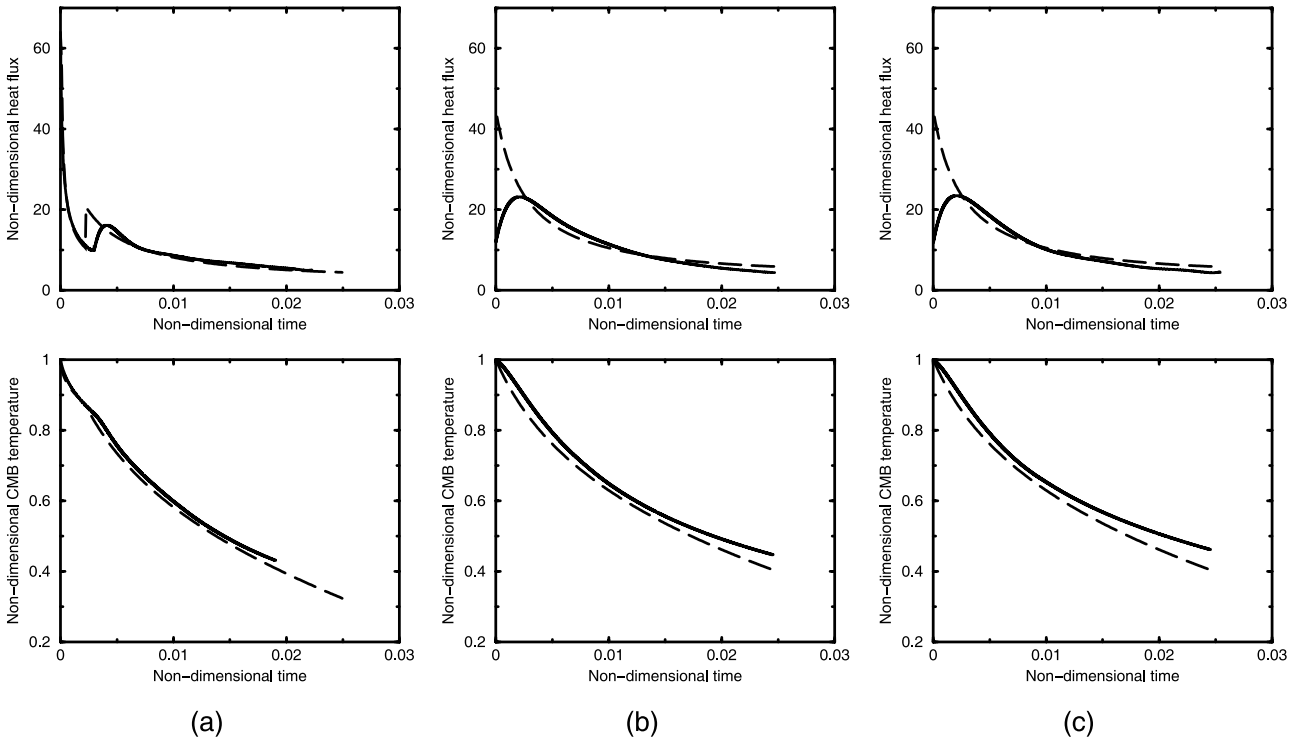

Figure 8. The CMB heat flux and CMB temperature as functions of time for the three cases shown in Figures 5, 6, and 7 (all parameters are nondimensional): (a) $h(0) \approx 0$, (b) 0.25, and (c) 0.5. The solid lines correspond to the 3-D numerical simulations. The dashed lines are parameterized convection calculations based on the stagnant lid convection scaling laws. An abrupt increase in the heat flux in Figure 8a is due to the onset of convection. In Figures 8b and 8c convection starts at $t = 0$. The difference between the 3-D simulations and parameterized convection calculations is due to a transient behavior which is not captured by the parameterized convection model.

superplume. Depending on the magnitude of mantle viscosity, the dimensional time scale for these stages can be quite broad ranging from millions to hundreds of millions of years [*Ke and Solomatov*, 2006].

[43] The process of superplume formation is discussed in detail by *Ke and Solomatov* [2004, 2006]. Superplumes form as a result of Rayleigh-Taylor-type instability due to the density contrast between the thermal boundary layer and the overlaying mantle. This happens at the time when the instability becomes faster than the expansion of the thermal boundary layer.

[44] Note that during the previous stage of evolution, when the thermal boundary layer at the base of the mantle was significantly molten the expansion of the thermal boundary layer was much faster than the development of the large-scale instability. After the rheological transition, the expansion of the TBL slows down by many orders of magnitude because the behavior of the boundary layer changes from liquid-like to solid-like. It is also worth noting for the initial values $h(0) = 0.25$ and 0.5 (Figures 6 and 7) the large-scale instability of the whole boundary layer is faster than the propagation of the boundary layer already at the beginning of simulations.

[45] Figure 8 shows the CMB temperature and the CMB heat flux (equation (11)) as functions of time for the three cases presented in Figures 5, 6, and 7. For comparison, we modeled this stage of evolution using parameterized convection approach based on equation (11). The parameterized convection calculations agree reasonably well with the three-dimensional finite element calculations despite the fact that the boundary layer is being swept away by the superplume. We interpret this agreement as an indication that the heat flux at the core-mantle boundary continues to be largely controlled by the rheological temperature scale ΔT_{rh}. Fluid dynamics of this regime is an important problem which would be interesting to address analytically. A mismatch in the beginning of evolution is due to a transient stage associated with the onset of convection. In the case of a negligibly small initial boundary layer thickness (Figure 8a), the parameterized convection calculations take into account the initial conductive cooling. In this case, convection starts after the critical conditions for the onset of convection are satisfied [*Solomatov and Moresi*, 2002; *Ke and Solomatov*, 2004, 2006]. For the two other cases (Figures 8b and 8c), the initial thickness of the boundary layer ($h(0) = 0.25$ and 0.5 correspondingly) is sufficiently large so that convection starts at the beginning of evolution.

5. Implications for the Early Martian Magnetism

[46] Present-day Mars has no global intrinsic magnetic field. However, strong crustal remnant magnetism discovered by Mars Global Surveyor suggests that Mars once possessed a dynamo early in its history (~4 Ga ago) [*Acuna et al.*, 1999; *Connerney et al.*, 1999]. The cessation time of dynamo is inferred from the absence of magnetic field at

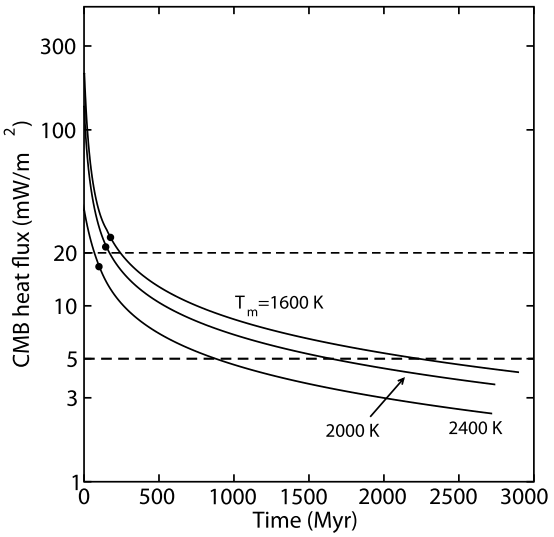

Figure 9. The CMB heat flux as a function of time during the superplume formation. Depending on the initial mantle temperature, small-scale convection in the partial melting boundary layer ceases around 100–150 million years (indicated by solid black circles) and after this the heat is transported across the boundary layer by conduction. The dashed lines show the range of the critical heat flux values for the cessation of the dynamo.

several large impact basins, which suggests that Mars did not have its magnetic field when these impacts happened [*Acuna et al.*, 1999]. Recent studies of giant buried basins [*Lillis et al.*, 2006, 2007a, 2007b] further constrain the cessation time of the dynamo to be 4.15–4.40 Ga ago if the cessation only happened once in the planetary history.

[47] Several models have been proposed that explain operation of dynamo in the early history of Mars [*Nimmo and Stevenson*, 2000; *Breuer and Spohn*, 2003; *Williams and Nimmo*, 2004]. Our model can generate a dynamo as well. During the first 10^2 years, when the bottom boundary layer is molten, the heat flux (Figure 2d) is many orders of magnitude higher than the critical heat flux $F_c \sim 5–20$ mW m^{-2} required for the dynamo [*Stevenson et al.*, 1983; *Nimmo and Stevenson*, 2000; *Williams and Nimmo*, 2004]. After the boundary layer crystallizes below the rheological transition, the heat flux drops significantly, yet it is sufficiently high to generate the dynamo for several hundred million years depending on model parameters (Figure 9). Note that small-scale convection in the boundary layer stops after 100–150 Ma and the subsequent evolution continues in the conductive regime. The long-term evolution (beyond 100–1000 Ma) can be affected by factors that are not considered in our model. In particular, if significant amounts of radiogenic isotopes are left in the mantle, the radiogenic heating would reduce the temperature contrast between the core and the mantle and decrease the duration time of the dynamo [*Nimmo and Stevenson*, 2000].

6. Conclusion

[48] We suggest a model of a coupled core-mantle evolution of early Mars assuming that the core was much hotter than the mantle. The evolution is divided into two stages. During the first stage, the thermal boundary layer at the base of the mantle is molten and convection within the boundary layer is controlled by liquid state viscosity. This stage is calculated using a parameterized convection approach. The time scale for the crystallization of the boundary layer from a completely molten state to melt fraction ~40% is of the order of 100 years. During this time, the mantle above the boundary layer is effectively stagnant. The boundary layer quickly expands upward, while its temperature and the temperature of the core decrease. The second stage of evolution, during which the bottom boundary layer crystallizes completely, is modeled using the three-dimensional finite element code CitcomS. Because the expansion of the thermal boundary layer becomes very slow, a large-scale instability of the boundary layer develops that eventually produces a superplume. This superplume continues to cool the core and generates sufficiently high heat flux that allows operation of the dynamo for at least several hundred million years.

[49] **Acknowledgments.** The authors would like to thank two anonymous reviewers and the Associate Editor for their thoughtful and constructive comments that helped to improve the manuscript. This work was supported by NASA grants NNX06AB05G and NNX07AQ74G.

References

Acuna, M. H., et al. (1999), Global distribution of crustal magnetization discovered by the Mars Global Surveyor MAG/ER experiment, *Science*, *284*, 790–793.

Anderson, O. L. (1995), Mineral physics of iron and of the core, *U.S. Natl. Rep. Int. Union Geod. Geophys. 1991–1994, Rev. Geophys.*, *33*, 429–441.

Boehler, R. (1996), Melting temperature of the Earth's mantle and core: Earth's thermal structure, *Annu. Rev. Earth Planet. Sci.*, *24*, 15–40.

Boehler, R. (2000), High-pressure experiments and the phase diagram of lower mantle and core materials, *Rev. Geophys.*, *38*, 221–245.

Breuer, D., and T. Spohn (2003), Early plate tectonics versus single-plate tectonics on Mars: Evidence from magnetic field history and crust evolution, *J. Geophys. Res.*, *108*(E7), 5072, doi:10.1029/2002JE001999.

Canup, R. M. (2004), Simulations of a late lunar-forming impact, *Icarus*, *168*, 433–456.

Chopelas, A. (1996), Thermal expansivity of lower mantle phases MgO and $MgSiO_3$ perovskite at high pressure derived from vibrational spectroscopy, *Phys. Earth Planet. Inter.*, *98*, 3–15.

Connerney, J. E. P., et al. (1999), Magnetic lineations in the ancient crust of Mars, *Science*, *284*, 794–798.

Connolly, J. A. D., and Y. Y. Podladchikov (2007), Decompaction weakening and channeling instability in ductile porous media: Implications for asthenospheric melt segregation, *J. Geophys. Res.*, *112*, B10205, doi:10.1029/2005JB004213.

Davaille, A., and C. Jaupart (1993a), Transient high Rayleigh number thermal convection with large viscosity variations, *J. Fluid Mech.*, *253*, 141–166.

Davaille, A., and C. Jaupart (1993b), Thermal convection in lava lakes, *Geophys. Res. Lett.*, *20*, 1827–1830.

Elkins-Tanton, L. T., E. M. Parmentier, and P. C. Hess (2003), Magma ocean fractional crystallization and cumulate overturn in terrestrial planets: Implications for Mars, *Meteorit. Planet. Sci.*, *38*, 1753–1771.

Elkins-Tanton, L. T., P. C. Hess, and E. M. Parmentier (2005a), Possible formation of ancient crust on Mars through magma ocean processes, *J. Geophys. Res.*, *110*, E12S01, doi:10.1029/2005JE002480.

Elkins-Tanton, L. T., S. E. Zaranek, E. M. Parmentier, and P. C. Hess (2005b), Early magnetic field and magmatic activity on Mars from magma ocean cumulate overturn, *Earth Planet. Sci. Lett.*, *236*, 1–12.

Fowler, A. C. (1985), Fast thermoviscous convection, *Stud. Appl. Math.*, *72*, 189–219.

Golabek, G. J., H. Schmeling, and P. J. Tackley (2008), Earth's core formation aided by flow channelling instabilities induced by iron diapirs, *Earth Planet. Sci. Lett.*, *271*, 348–358.

Hofmeister, A. M. (1999), Mantle values of thermal conductivity and the geotherm for phonon lifetimes, *Science*, *283*, 1699–1706.

Karato, S.-I., and P. Wu (1993), Rheology of the upper mantle: A synthesis, *Science*, *260*, 771–778.

Ke, Y., and V. S. Solomatov (2004), Plume formation in strongly temperature-dependent viscosity fluids over a very hot surface, *Phys. Fluids*, *16*, 1059–1063.

Ke, Y., and V. S. Solomatov (2006), Early transient superplumes and the origin of the Martian crustal dichotomy, *J. Geophys. Res.*, *111*, E10001, doi:10.1029/2005JE002631.

Kraichnan, R. H. (1962), Turbulent thermal convection at arbitrary Prandtl number, *Phys. Fluids*, *5*, 1374–1389.

Labrosse, S., J. W. Hernlund, and N. Coltice (2007), A crystallizing dense magma ocean at the base of the Earth's mantle, *Nature*, *450*, 866–869.

Landau, L. D., and E. M. Lifshitz (1987), *Fluid Mechanics*, Pergamon, New York.

Liebske, C., B. Schmickler, H. Terasaki, B. T. Poe, A. Suzuki, K.-I. Funakoshi, R. Ando, and D. C. Rubie (2005), Viscosity of peridotite liquid up to 13 GPa: Implications for magma ocean viscosities, *Earth Planet. Sci. Lett.*, *240*, 589–604.

Lillis, R. J., H. V. Frey, M. Manga, D. L. Mitchell, R. P. Lin, and M. H. Acuna (2006), Bracketing the end of the Martian dynamo: The ages and magnetic signatures of Hellas and Ladon basins, *Lunar Planet. Sci.*, *XXXVII*, Abstract 2183.

Lillis, R. J., H. V. Frey, M. Manga, D. L. Mitchell, R. P. Lin, and M. H. Acuna (2007a), Basin magnetic signatures and crater retention ages: Evidence for a rapid shutdown of the Martian dynamo, *Lunar Planet. Sci.*, *XXXVIII*, Abstract 1515.

Lillis, R. J., H. V. Frey, M. Manga, D. L. Mitchell, R. P. Lin, and M. H. Acuna (2007b), Magnetic signatures and crater retention ages of giant buried basins on Mars; new constraints on the timing of the ancient dynamo, in *Seventh International Conference on Mars, July 9–13, 2007, Pasadena CA* [CD-ROM], *LPI Contrib., 1353*, Abstract 3090.

Longhi, J., E. Knittle, J. R. Holloway, and H. Wanke (1992), The bulk composition, mineralogy and internal structure of Mars, in *Mars*, edited by H. H. Kieffer et al., pp. 184–208, Univ. of Ariz. Press, Tucson.

Moresi, L.-N., and V. S. Solomatov (1995), Numerical investigation of 2D convection with extremely large viscosity variations, *Phys. Fluids*, *7*, 2154–2162.

Morris, S., and D. Canright (1984), A boundary layer analysis of Bénard convection in a fluid of strongly temperature dependent viscosity, *Phys. Earth Planet. Inter.*, *36*, 355–373.

Mound, J., and B. Buffett (2007), Viscosity of the Earth's fluid core and torsional oscillations, *J. Geophys. Res.*, *112*, B05402, doi:10.1029/2006JB004426.

Nimmo, F., and D. J. Stevenson (2000), Influence of early plate tectonics on the thermal evolution and magnetic field of Mars, *J. Geophys. Res.*, *105*, 11,969–11,979.

Reese, C. C., and V. S. Solomatov (2006), Fluid dynamics of local Martian magma oceans, *Icarus*, *184*, 102–120.

Roscoe, R. (1952), The viscosity of suspensions of rigid spheres, *Br. J. Appl. Phys.*, *3*, 267–269.

Schubert, G., D. L. Turcotte, and P. Olson (2001), *Mantle Convection in the Earth and Planets*, 940 pp., Cambridge Univ. Press, New York.

Scott, T. J., and D. L. Kohlstedt (2004), The effect of large melt fraction on the deformation behavior of peridotite: Implications for the viscosity of IO's mantle and the rheologically critical melt fraction, *Eos Trans. AGU*, *85*(47), Fall Meet. Suppl., Abstract 4582.

Siggia, E. D. (1994), High Rayleigh number convection, *Annu. Rev. Fluid Mech.*, *26*, 137–168.

Solomatov, V. S. (1995), Scaling of temperature- and stress-dependent viscosity convection, *Phys. Fluids*, *7*, 266–274.

Solomatov, V. S. (2000), Fluid dynamics of a terrestrial magma ocean, in *Origin of the Earth and Moon*, edited by R. Canup and K. Righter, pp. 323–338, Univ. Ariz. Press, Tucson.

Solomatov, V. S. (2007), Magma oceans and primordial mantle differentiation, in *Treatise on Geophysics*, vol. 9, edited by G. Schubert, pp. 91–120, Elsevier, Amsterdam.

Solomatov, V. S., and L.-N. Moresi (2000), Scaling of time-dependent stagnant lid convection: Application to small-scale convection on the Earth and other terrestrial planets, *J. Geophys. Res.*, *105*, 21,795–21,818.

Solomatov, V. S., and L.-N. Moresi (2002), Small-scale convection in the D″ layer, *J. Geophys. Res.*, *107*(B1), 2016, doi:10.1029/2000JB000063.

Solomatov, V. S., and D. J. Stevenson (1993a), Nonfractional crystallization of a terrestrial magma ocean, *J. Geophys. Res.*, *98*, 5391–5406.

Solomatov, V. S., and D. J. Stevenson (1993b), Kinetics of crystal growth in a terrestrial magma ocean, *J. Geophys. Res.*, *98*, 5407–5418.

Solomon, S. (1979), Formation, history and energetics of cores in the terrestrial planets, *Phys. Earth Planet. Inter.*, *19*, 168–182.

Stevenson, D. J. (2001), Mars' core and magnetism, *Nature*, *412*, 214–219.

Stevenson, D. J., T. Spohn, and G. Schubert (1983), Magnetism and thermal evolution of the terrestrial planets, *Icarus*, *54*, 466–489.

Trompert, R. A., and U. Hansen (1998), On the Rayleigh number dependence of convection with a strongly temperature-dependent viscosity, *Phys. Fluids*, *10*, 351–360.

Wiggins, C., and M. Spiegelman (1995), Magma migration and magmatic solitary waves in 3-D, *Geophys. Res. Lett.*, *22*, 1289–1292.

Williams, J.-P., and F. Nimmo (2004), Thermal evolution of the Martian core: Implications for an early dynamo, *Geology*, *37*, 97–100.

Williams, Q. (1998), The temperature contrast across D″, in *The Core-Mantle Boundary Region*, *Geodyn. Ser.*, vol. 28, edited by M. Gurnis et al., pp. 73–81, AGU, Washington, D. C.

Yoder, C. F., A. S. Konopliv, D. N. Yuan, E. M. Standish, and W. M. Folkner (2003), Fluid core size of Mars from detection of the solar tide, *Science*, *300*, 299–303.

Zhang, J., and C. Herzberg (1994), Melting experiments on anhydrous peridotite KLB-1 from 5.0 to 22.5 GPa, *J. Geophys. Res.*, *99*, 17,729–17,742.

Zharkov, V. N. (1986), *Interior Structure of the Earth and Planets*, Harwood, New York.

Zhong, S. J., M. T. Zuber, L. Moresi, and M. Gurnis (2000), Role of temperature-dependent viscosity and surface plates in spherical shell models of mantle convection, *J. Geophys. Res.*, *105*, 11,063–11,082.

Y. Ke and V. S. Solomatov, Department of Earth and Planetary Sciences, Washington University, Campus Box 1169, St. Louis, MO 63130, USA. (yke@levee.wustl.edu)